microorganisms

MDPI

Article

Diffusional Interactions among Marine Phytoplankton and Bacterioplankton: Modelling H_2O_2 as a Case Study

Naaman M. Omar [1], Ondřej Prášil [2], J. Scott P. McCain [3] and Douglas A. Campbell [1,*]

[1] Department of Biology, Mount Allison University, Sackville, NB E4L1G7, Canada; nomar@mta.ca
[2] Center Algatech, Laboratory of Photosynthesis, Novohradska 237, CZ 37981 Trebon, Czech Republic; prasil@alga.cz
[3] Department of Biology, Massachusetts Institute of Technology, Boston, MA 02142, USA; smccain@mit.edu
* Correspondence: dcampbel@mta.ca

Abstract: Marine phytoplankton vary widely in size across taxa, and in cell suspension densities across habitats and growth states. Cell suspension density and total biovolume determine the bulk influence of a phytoplankton community upon its environment. Cell suspension density also determines the intercellular spacings separating phytoplankton cells from each other, or from co-occurring bacterioplankton. Intercellular spacing then determines the mean diffusion paths for exchanges of solutes among co-occurring cells. Marine phytoplankton and bacterioplankton both produce and scavenge reactive oxygen species (ROS), to maintain intracellular ROS homeostasis to support their cellular processes, while limiting damaging reactions. Among ROS, hydrogen peroxide (H_2O_2) has relatively low reactivity, long intracellular and extracellular lifetimes, and readily crosses cell membranes. Our objective was to quantify how cells can influence other cells via diffusional interactions, using H_2O_2 as a case study. To visualize and constrain potentials for cell-to-cell exchanges of H_2O_2, we simulated the decrease of [H_2O_2] outwards from representative phytoplankton taxa maintaining internal [H_2O_2] above representative seawater [H_2O_2]. [H_2O_2] gradients outwards from static cell surfaces were dominated by volumetric dilution, with only a negligible influence from decay. The simulated [H_2O_2] fell to background [H_2O_2] within ~3.1 µm from a *Prochlorococcus* cell surface, but extended outwards 90 µm from a diatom cell surface. More rapid decays of other, less stable ROS, would lower these threshold distances. Bacterioplankton lowered simulated local [H_2O_2] below background only out to 1.$_2$ µm from the surface of a static cell, even though bacterioplankton collectively act to influence seawater ROS. These small diffusional spheres around cells mean that direct cell-to-cell exchange of H_2O_2 is unlikely in oligotrophic habits with widely spaced, small cells; moderate in eutrophic habits with shorter cell-to-cell spacing; but extensive within phytoplankton colonies.

Keywords: diffusional interactions; hydrogen peroxide; phytoplankton; bacterioplankton

Citation: Omar, N.M.; Prášil, O.; McCain, J.S.P.; Campbell, D.A. Diffusional Interactions among Marine Phytoplankton and Bacterioplankton: Modelling H_2O_2 as a Case Study. *Microorganisms* **2022**, *10*, 821. https://doi.org/10.3390/microorganisms10040821

Academic Editor: Katherina Petrou

Received: 7 February 2022
Accepted: 13 April 2022
Published: 15 April 2022

1. Introduction

1.1. Marine Phytoplankton

Phytoplankton are a polyphyletic functional grouping of ~275,000 species of oxygenic photosynthetic microorganisms that grow while suspended in marine or freshwater habitats [1,2]. Phytoplankton interact with their aqueous environment [3], and with co-occurring bacterioplankton cells, through diffusion of nutrients, toxic compounds and signaling molecules, notably including reactive oxygen species (ROS). Phytoplankton span a wide size range [4] (Table 1), which directly affects their diffusional interactions. Larger cells have longer paths for intracellular diffusion or transport paths for solutes, and can therefore potentially impose larger concentration gradients between their internal cell contents and the local microenvironment. Larger cells also have lower surface to volume ratios which impose limits on their trans-membrane transport per biovolume of the cell [5].

On the other hand, some larger cells have dynamic control over their sinking through water, and can thereby refresh their surface boundary layers more effectively than can smaller cells [3,6].

1.2. Phytoplankton Cell Spacing in Oceans

Phytoplankton and bacterioplankton cell numbers in the ocean vary widely, and therefore so does intercellular distance (Table 1). Direct colonization of phytoplankton by bacteria [7], or colony-forming phytoplankters, bring multiple cells into yet closer local proximities. For example, within *Phaeocystis* colonies, cell densities reach 2.4×10^7 cells mL^{-1} [8] (Table 1).

Table 1. Phytoplankton and bacterioplankton cell sizes and representative suspension densities.

Habitat	Taxa	Metabolism	Cell m^{-3}	Cell Radius µm	Citation
Oligotrophic	Bacterioplankton	Hetero	4.7×10^{10}	0.5	[9]
Oligotrophic	Bacterioplankton	Hetero	2.0×10^{11}	0.5	[10]
Oligotrophic	Diatoms	Phyto	5.6×10^{7}	10.0	[11]
Oligotrophic	Dinoflagellates	Phyto	6.5×10^{6}	10.0	[11]
Oligotrophic	PicoEukaryotes	Phyto	6.7×10^{8}	2.0	[12]
Oligotrophic	PicoEukaryotes	Phyto	2.0×10^{9}	2.0	[10]
Oligotrophic	Prochlorococcus	Phyto	4.7×10^{10}	0.3	[12]
Oligotrophic	Prochlorococcus	Phyto	3.8×10^{10}	0.3	[10]
Oligotrophic	Silicoflagellates	Phyto	1.3×10^{7}	10.0	[11]
Oligotrophic	Synechococcus	Phyto	3.0×10^{9}	1.0	[12]
Oligotrophic	Synechococcus	Phyto	2.0×10^{9}	1.0	[10]
Mesotrophic	Bacterioplankton	Hetero	3.3×10^{11}	0.5	[10]
Mesotrophic	PicoEukaryotes	Phyto	3.0×10^{9}	2.0	[10]
Mesotrophic	Prochlorococcus	Phyto	3.1×10^{10}	0.3	[10]
Mesotrophic	Synechococcus	Phyto	6.0×10^{9}	1.0	[10]
Eutrophic	Bacterioplankton	Hetero	4.6×10^{11}	0.5	[10]
Eutrophic	Bacterioplankton	Hetero	4.6×10^{13}	0.5	[13]
Eutrophic	Chlorophytes	Phyto	8.2×10^{10}	2.5	[14]
Eutrophic	Chroococcales	Phyto	8.2×10^{10}	1.0	[14]
Eutrophic	Cyanobium	Phyto	4.0×10^{12}	1.0	[14]
Eutrophic	PicoEukaryotes	Phyto	3.0×10^{9}	2.0	[10]
Eutrophic	PicoEukaryotes	Phyto	1.5×10^{13}	2.0	[13]
Eutrophic	Synechococcus	Phyto	4.5×10^{9}	1.0	[10]
Colony	Cyanobium	Phyto	1.0×10^{13}	1.0	[14]
Colony	Phaeocystis	Phyto	2.4×10^{13}	2.2	[8]

These wide ranges of cell suspension densities for phytoplankton and bacterioplankton across habitats strongly influence the extent to which the growth and activity of a phytoplankton population or community alters, or even governs, solute concentrations in the local habitat [15–18]. Beyond the bulk activities of the phytoplankton population or community, differences in cell suspension densities mean the diffusional path lengths for solutes separating individual cells vary by orders of magnitude across habitats and taxa. Intercellular distances then influence whether the activity of an individual cell can directly influence the microenvironment of neighboring cells [19].

Our understanding of the taxa- and habitat-specific effects of cell-to-cell separation is then influenced by schematic visualizations of phytoplankton communities with implied cell suspension densities far higher than is realistic, or with cell symbol sizes scaled differently than the scaling of the spatial axes [20]. Symbol size scaling exaggerated relative to the scaling of the spatial axes allows schematic visualizations of cells, but can give a visual impression of a community with fairly close cell-to-cell interactions. In our visualizations, we maintain cell symbol size at the same size scaling as the spatial axes (Figure 1).

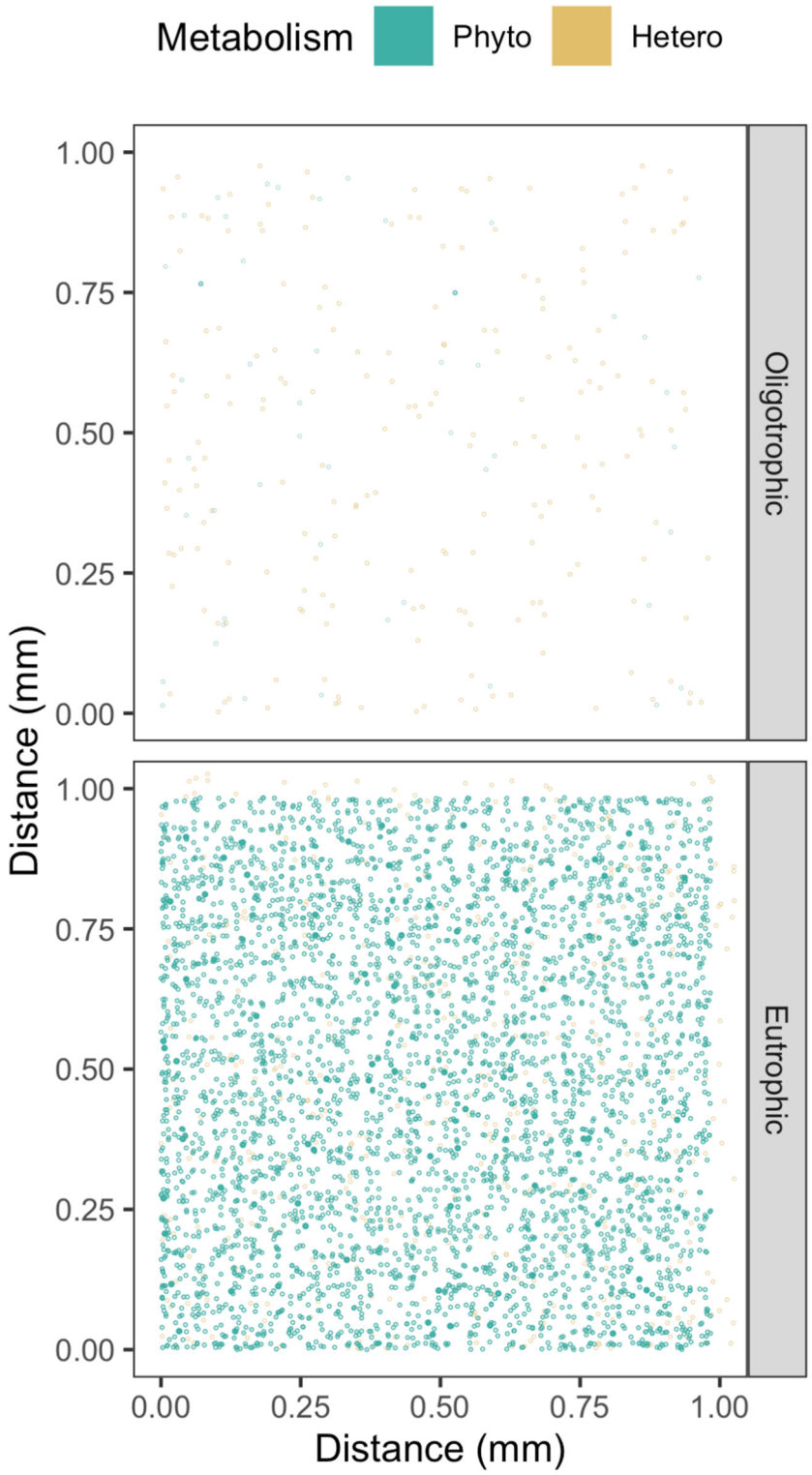

Figure 1. Phytoplankton and heterotrophic bacteria spacing from eutrophic or oligotrophic environments, with cell size on the same scaling as the 1 mm XY spatial axes. A 1 mm Z spatial axis is coded with fainter points farther back.

1.3. Reactive Oxygen Species

Electrons can transfer from photosynthetic or respiratory electron transport to reduce O_2 to form the superoxide radical, a reactive oxygen species (ROS) [21,22] (Reaction (1)).

ROS include both radicals (superoxide, nitric oxide and hydroxyl radicals) and non-radicals (hydrogen peroxide, singlet oxygen and peroxynitrite), which are more reactive than ground state di-oxygen molecules [23,24]. Reduction of O_2 to H_2O requires the sequential addition of four electrons, and therefore progresses through three ROS intermediates: superoxide ($O_2^{\bullet -}$), hydrogen peroxide (H_2O_2) and hydroxyl radical ($OH^{\bullet}$) (Reaction (1)) [25]. ROS are by-products of both photosynthetic and heterotrophic metabolism, but are also generated abiotically in seawater [26].

$$\begin{gathered} O_2 + e^- \rightarrow O_2^{\bullet -} \\ O_2^{\bullet -} + 2H^+ + e^- \rightarrow H_2O_2 \\ H_2O_2 + H^+ + e^- \rightarrow H_2O + OH^{\bullet} \\ OH^{\bullet} + e^- + H^+ \rightarrow H_2O \end{gathered} \quad (1)$$

Biogenic production of extracellular ROS mediated by microorganisms is a significant contributor to marine environments [27,28], mediated by taxa ranging from heterotrophic bacteria to diatoms including those from the *Thalassiosira* and *Coscinodiscus* genera [28–35].

ROS are important at low concentrations due to their role in cell signaling [36–42] and lipid accumulation [43]. In order to benefit from ROS, organisms must maintain ROS levels above the cytostatic threshold, the minimum concentration of ROS required to maintain normal cellular processes, as well as below the cytotoxic threshold, the level at which the negative effects of ROS outweigh the positives [44].

1.4. Concentrations and Properties of H_2O_2

H_2O_2 is an uncharged compound documented in the ocean at concentrations of 10^{-9} to 10^{-6} mol L^{-1} [29,45] depending upon location and conditions. These [H_2O_2] are high enough to significantly contribute to the redox cycling of copper [46,47]. [H_2O_2] in seawater increases after precipitation, including rain and snowfall [18,26,48]. [H_2O_2] in seawater also follows a diurnal cycle with a peak at mid-day [18,49,50], which suggests significant direct or indirect photochemical or photobiological generation of H_2O_2. [H_2O_2] also exhibits latitudinal variation at the surface, higher in the brighter, warmer, mid to low latitudes compared to the colder, darker, higher latitudes [50]. The authors of [50] suggest that regional variation in [H_2O_2] may be caused by the depth of the mixed layer and the concentration of total dissolved organic carbon. Abiotic production rates of H_2O_2 vary from 0.28 to 4.2 pM s^{-1} in near surface open ocean waters vs. 1.0 to 84.4 pM s^{-1} in coastal sites [26].

The diffusion coefficients (a measure of how quickly a molecule travels via diffusion), and therefore the diffusional mobilities, of ROS through seawater vary widely. Diffusion coefficients in water decrease with increasing molecular mass, and from uncharged to charged compounds. Diffusion coefficients are strongly influenced by temperature and slightly influenced by pressure. For H_2O_2 at ~20 °C the diffusion coefficient is ~1500 μm^2 μs^{-1} (note conversion of units from more typical reporting of cm^2 s^{-1}) [51]. In aquatic systems, H_2O_2 has extracellular lifetimes of hours to days [29,52] before decay.

H_2O_2 is acutely toxic to most cells in the range of 10^{-5} to 10^{-4} mol L^{-1} range [53], about 10-fold higher than seawater concentrations [29,45]. We found few quantitative estimates of the intracellular concentrations of H_2O_2 within cells [54–60], with a particular lack of measurements from phytoplankton. Limited data, from mammalian cells, support an intracellular H_2O_2 concentration of 10^{-6} M [61]. Although only weakly directly reactive, H_2O_2 can react with thiols and methionine [62] and thereby modulate gene expression and transcription [63,64]. Meanwhile, limited experimental data indicate that heterotrophic bacteria maintain an internal [H_2O_2] of 1/10 of the external [H_2O_2] when extracellular H_2O_2 is present [58,60], as it is in seawater. The authors of [58] also predicted an intra-

cellular steady-state [H_2O_2] of 20 nM in the absence of extracellular H_2O_2, which is far below the toxic threshold of intracellular H_2O_2 [60], and is likely for the maintenance of physiological roles of H_2O_2. Cytotoxic effects of H_2O_2, including lipid damage, are primarily caused by H_2O_2 converting to the hydroxyl radical, which is strongly oxidative [52]. Interestingly, H_2O_2 may be used as a terminal electron acceptor in the absence of oxygen in *Escherichia coli* [65].

H_2O_2 readily crosses the cell membrane [53] primarily through aquaporins [66–69]. As a result, intracellular H_2O_2 exchanges with extracellular H_2O_2, but cells can nevertheless maintain intracellular [H_2O_2] significantly different than extracellular [H_2O_2] [58]. Other ROS rarely cross cell membranes and therefore the intra- and extracellular pools are not directly connected, although they may influence each other indirectly through transformations to other ROS, for example dismutation of intracellular $O_2^{\bullet-}$ to form intracellular H_2O_2 which can then exchange with extracellular H_2O_2, and vice versa.

A significant fraction of H_2O_2 destruction in aqueous systems may be attributed to the activities of heterotrophic microbes [70], although heterotrophs are minor contributors to bulk [H_2O_2]. Microbial scavenging of H_2O_2 indeed increases the survival of *Prochlorococcus* through extended periods of darkness, as demonstrated through co-culture studies [71] with 'helper' bacteria which carry genes for catalase. In the open ocean, bulk [H_2O_2] levels generally remain below the cytotoxic threshold, partly because heterotrophic organisms provide catalase [72].

Changes in [H_2O_2], or other ROS, around a cell will depend upon net production, or consumption by the cell, which generate net release (or uptake) of [H_2O_2] from the cell after any intracellular or cell-associated scavenging. These inputs can interact to generate a diffusion-generated gradient of [H_2O_2] around the cell, above or below seawater [H_2O_2]. Whether or not a cell establishes a zone of [H_2O_2] different from the [H_2O_2] background also depends upon extracellular destruction and diffusion rates. The extent of this altered zone will then influence downstream processes. For specific cell–cell interactions or responses, a cell has to change the [H_2O_2] in the local microenvironment sufficiently to provoke a response in neighboring cells. Beyond this local sphere of influence around an individual cell, the collective activity of cells in a community contributes to generating a general seawater [H_2O_2], which in turn influences cellular gene expression and metabolism.

1.5. Goals

Microbes consume and produce H_2O_2, thereby potentially helping, or at least influencing, other microbes. We sought to quantify the influences of cell density and cell size on these potential microbial interactions. H_2O_2 presents a good case study for diffusional interactions among microbes. H_2O_2 readily traverses cell membranes, and there is information on background concentrations of H_2O_2 in seawater, H_2O_2 diffusion coefficients in seawater and some estimates of cellular concentrations of H_2O_2, as either absolute values or ratios compared to external [H_2O_2]. We can therefore approximate concentration gradients generated by [H_2O_2] diluting outwards from a cell maintaining a homeostatic intracellular [H_2O_2] higher than seawater [H_2O_2], or the concentration gradient inwards towards a hypothetical cell maintaining a homeostatic intracellular [H_2O_2] lower than seawater [H_2O_2]. We can use these simple approximations to generate quantitative thresholds for when H_2O_2 released from a cell can directly influence neighboring cells, i.e., how much, and how far, a phytoplankton or bacterioplankton cell can change the local [H_2O_2].

2. Results and Discussion

2.1. Cell to Cell Spacing across Habitats and Taxa

Possible cell-to-cell exchanges of H_2O_2 are mediated by diffusions through intercellular path lengths, varying by orders of magnitude across habitats and taxa. To understand such diffusional exchanges we need realistic visualizations of cell spacings, achieved by maintaining cell symbol size at the same size scaling as the spatial axes (Figure 1). In the visualization of randomized cell spacing under oligotrophic conditions, we see wide

spacing among cells, because the small cell symbols are on the same size scaling as the spatial axes. In the visualization of randomized cell spacing under eutrophic conditions, some cells are in close proximity. Note that this standardized scaling visualization approach is only feasible with highly expanded spatial axes such as the 1 mm axis used in Figure 1, equivalent to simulation of only 1 µL. Attempting to visualize 10 mm axes, equivalent to a 1 mL volume, causes the cell symbol size to shrink below visibility (data not presented). A further nuance not captured in these visualizations and subsequent simulations is non-random clustering of cells, as perhaps around particles of marine snow.

2.2. H_2O_2 Concentration Gradients around Cells

Figure 2 shows a light blue background for the approximate range of natural [H_2O_2] in seawater, with the simulated profiles of [H_2O_2] moving outward from a 'Bacterioplankton' cell with intracellular [H_2O_2] maintained below seawater [H_2O_2]; or outward from small phytoplankton cells of different sizes with intracellular [H_2O_2] maintained at 1 µmol L^{-1} [57], near the highest concentrations expected for seawater [ROS]. For [H_2O_2] generators (nominally, phytoplankton of different sizes), [H_2O_2] concentrations are highest near the cell surface and decrease with distance outwards. For [H_2O_2] consumers (nominally, bacterioplankton), [H_2O_2] concentrations are lowest near the cell surface.

Decay is a key influence on the pseudo-steady state bulk [H_2O_2] in seawater, but for our conceptual estimates of [H_2O_2] changing within the local region of the cell, the dilution term (black points, Figure 2) dominates the concentration gradient moving out from the cell. Including the influence of the decay term (red points, Figure 2) has only a negligible influence on [H_2O_2] moving out from the phytoplankton cell over simulated timescales of <100 µs and distances of ~100 µm. For other, less stable ROS, decay would become a significant influence, acting to narrow the local concentration gradients around cells.

Seawater contains H_2O_2 which varies significantly depending upon conditions and region. At some threshold distance out from the cell-specific sphere of influence upon local [ROS], it reaches the seawater [H_2O_2] (Figure 2), beyond which distance net [H_2O_2] production or consumption by the specific cell has no local influence on [H_2O_2], but is simply one input into the wider seawater [H_2O_2]. All other factors being equal, in our estimations the region over which a cell changes the local [H_2O_2] away from seawater [H_2O_2] increases with cell radius. This wider influence of cells with larger cell radii results primarily from the volume of the intracellular homeostatic [H_2O_2] increasing as the cube of cellular radius (Figure 2).

In this simple estimate, a heterotrophic bacterioplankton cell maintaining intracellular [H_2O_2] at 1/10 of the external seawater [H_2O_2] locally drops [H_2O_2] below the lower end of the seawater [H_2O_2] for a radius of only 1.2 µm. If the bacterioplankton cell were to maintain an intracellular [H_2O_2] of <1/10 of the external seawater [H_2O_2], the threshold distances would be greater. The phytoplankton cells maintaining intracellular [H_2O_2] at 1 µmol L^{-1} influence local [H_2O_2] above a low background level of seawater [H_2O_2] for radii of 3.1 µm for *Prochlorococcus* up to 90 µm for diatoms, or even more for yet larger phytoplankters not simulated. Furthermore, these threshold distances apply to the lowest published estimates for seawater [H_2O_2]. Under environments with higher seawater [H_2O_2], the threshold distances would be smaller.

2.3. Visualizing Cell to Cell Exchange of [H_2O_2]

We next combine our visualizations of cell suspensions from eutrophic, oligotrophic, or colonial habitats, overlaid with the mathematical expressions of cell-specific spheres of [H_2O_2] above or below seawater levels, to visualize the extent to which cells directly influence the [H_2O_2] environments of their neighbors.

In eutrophic habitats, bacterioplankters are numerous, but their small cell size, and correspondingly small cell-specific spheres of upon local [H_2O_2], mean that their individual contributions towards local [H_2O_2] are negligible (Figure 3), even though their collective influence upon background [H_2O_2] may be considerable [71,72]. Phytoplankton cells,

particularly the larger taxa, can however influence local [H_2O_2] over wider distances, leading to overlaps in their cell-specific spheres of influence (Figure 3) with bacterioplankton and with other phytoplankton, and opening the possibility of direct cell-to-cell signaling or cell-to-cell metabolic influences through [H_2O_2], beyond contributions to background seawater [H_2O_2]. In oligotrophic habitats, wider cell-to-cell spacings, and generally smaller cell sizes, make direct cell-to-cell reciprocal influences upon local [H_2O_2] unlikely, although the phytoplankton and bacterioplankton as a whole indeed contribute to establishment of the background [H_2O_2].

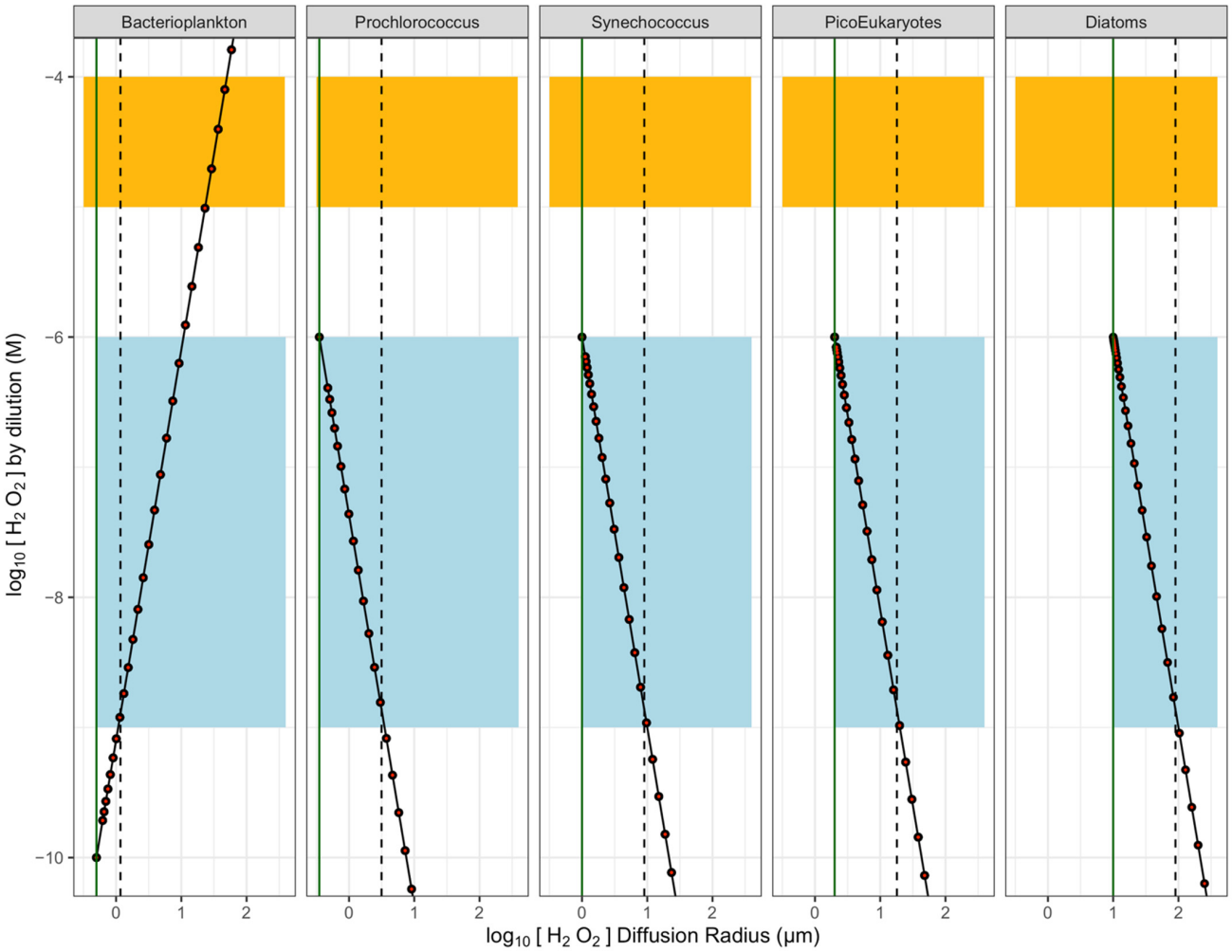

Figure 2. Estimates of concentration gradients of [H_2O_2] vs. distance outwards from 'heterotrophic' Bacterioplankton cell maintaining an internal [H_2O_2] below seawater background [H_2O_2] (blue band); or outwards from 'Phytoplankton' cells of different radii, maintaining an internal [H_2O_2] equal to 1/10 the cytotoxic threshold for [H_2O_2]. Orange indicates cytotoxic concentration range for [H_2O_2] (1×10^{-5} to 1×10^{-4} M). Black points show modelled [H_2O_2] under the influence of dilution alone. Red points show modelled [H_2O_2] under superimposed influences of dilution and (negligible) decay of H_2O_2. Vertical green lines indicate the cell surface. Vertical dashed lines indicate threshold radii out from cells, where [H_2O_2] around the cell falls or rises to seawater background levels. Beyond that threshold, the cell has no specific, local influence upon seawater [H_2O_2].

For phytoplankters growing colonially, the [H_2O_2] leaving specific cells within the colony strongly influence the local [H_2O_2] environments of neighboring cells in the colony (Figure 4). Such a colony could also be usefully simulated as a single homeostatic sphere of [H_2O_2], with a significant local sphere of influence beyond the colony. Although we did not include bacteria in Figure 4, in fact *Phaeocystis antarctica* colonies have rich bacterial

components [73], which may greatly alter the local H_2O_2 environment within the colony, beyond the activities of the *Phaeocystis* cells.

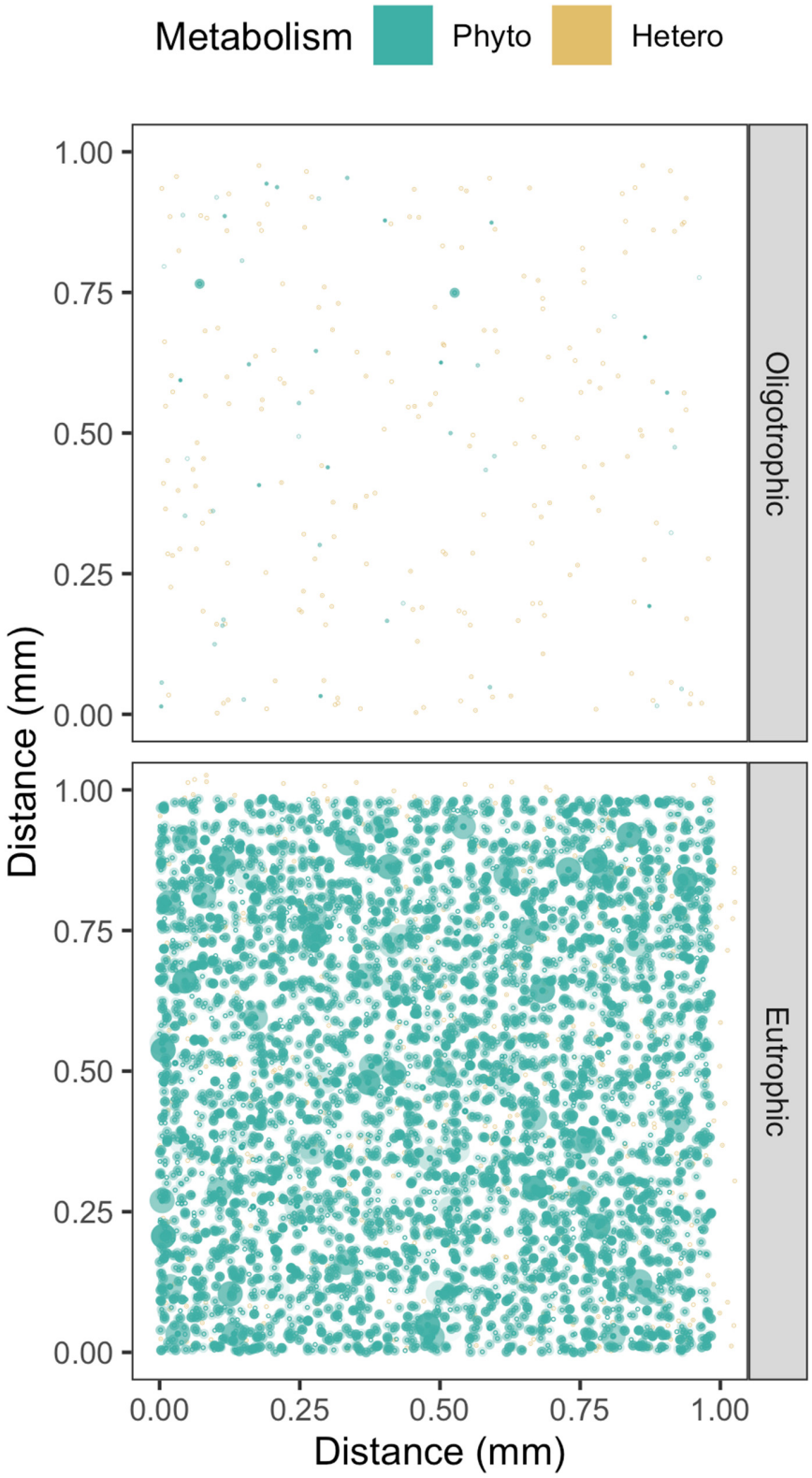

Figure 3. Simulations of $[H_2O_2]$ above seawater $[H_2O_2]$ (pale blue) out from Phytoplankton cells (green spheres, spanning a size range), or $[H_2O_2]$ below seawater $[H_2O_2]$ out from Bacterioplankton cells (red spheres, single nominal cell size). Cell position along a third Z axis is simulated by the 'alpha' with lighter cells further back.

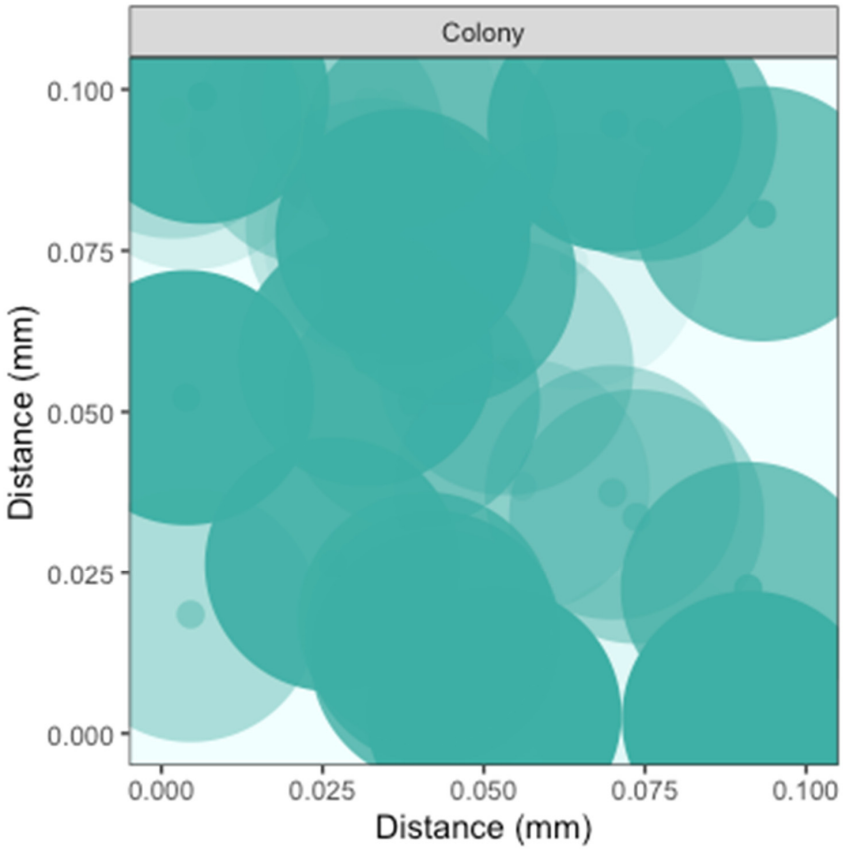

Figure 4. Simulation of $[H_2O_2]$ above seawater $[H_2O_2]$ within a Phaeocystis colony. Note the expansion of the axes scales to 0.1 mm. Cell position along a third Z axis is simulated by the 'alpha' with lighter cells further back.

2.4. Threshold Distances for Cell to Cell Exchange of $[H_2O_2]$

We find that cell size, cell suspension density, cellular $[H_2O_2]$ and seawater $[H_2O_2]$ interact to influence the potential for direct cell-to-cell diffusional interactions. We sought to generalize the estimations presented earlier for combinations of taxa x habitat (Figure 3) to summarize how these variables potentially affect cell-to-cell interactions via H_2O_2 (Figure 5).

Figure 5 plots combinations of cell suspension density (X axis, governing cell-to-cell distance), and the radii of the cell-specific sphere of influence upon $[H_2O_2]$ exceeding seawater $[H_2O_2]$ (Y axis), for homogeneous populations. The threshold lines mark the transition for cell-to-cell interactions, for four different ratios of cellular $[H_2O_2]$ to seawater $[H_2O_2]$. The areas above the threshold lines show the regions of cell radius and cell suspension density where the cell-specific spheres of influence upon $[H_2O_2]$ exceed the average cell-to-cell spacing, for a given ratio of cellular $[H_2O_2]$ to seawater $[H_2O_2]$. For the purpose of presentation, we collapsed cellular $[H_2O_2]$ and seawater $[H_2O_2]$ to the ratio of cellular $[H_2O_2]$ to seawater $[H_2O_2]$ since that ratio determines the position of the threshold line, rather than the absolute values for cellular $[H_2O_2]$ and seawater $[H_2O_2]$. We see that a homogeneous population of large cells of 40 µm radius would maintain overlapping cell-specific spheres of influence down to cell suspension densities of 2.7×10^9 cells m^3 (Figure 5). In contrast, a homogeneous population of cells of 0.5 µm radius would only achieve directly interacting cell-specific spheres of influence at a hypothetical 1.9×10^{15} cells m^3, far above cell suspension densities for most marine habitats (Table 1). For comparison, in Figure 5 we overlay symbols for representative taxa from different habitats (Table 1) showing that for hypothetical homogeneous populations the cell-specific spheres of influence are generally far below the expected cell-to-cell spacing.

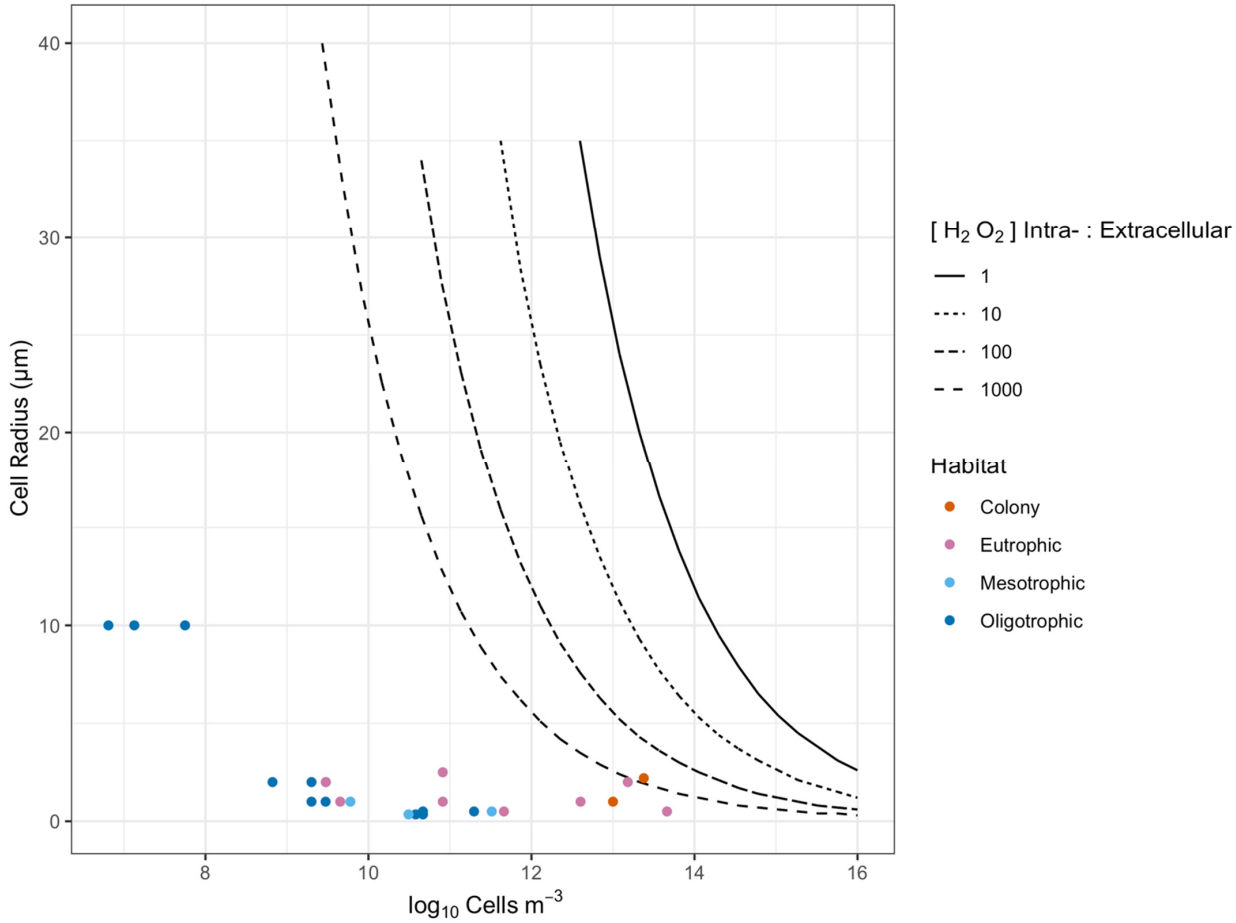

Figure 5. Thresholds for direct phytoplankton cell-to-cell interaction through $[H_2O_2]$ above seawater background. The X axis shows a range of cell m^{-3} (which in turn governs cell-to-cell distances), while the Y axis shows radii for cell-specific spheres of influence upon $[H_2O_2]$ (a function of cell size, intracellular $[H_2O_2]$ and seawater $[H_2O_2]$). The areas below the threshold lines show combinations where phytoplankton cell-to-cell distance exceeds the cell-specific $[H_2O_2]$ distance, so direct cell-to-cell interactions mediated by $[H_2O_2]$ are unlikely. The area above the threshold lines show combinations where phytoplankton cell-to-cell distance is less than the cell-specific $[H_2O_2]$ distance, so direct cell-to-cell interactions mediated by $[H_2O_2]$ are feasible. The four threshold lines refer to a range of ratios of phytoplankton intracellular to extracellular $[H_2O_2]$. Data points from different habitats show that direct phytoplankton cell-to-cell interactions are likely only within the Phaeocystis colony, whereas single phytoplankton cells are generally too small or too distant for direct interactions.

Figure 6 shows that for natural population densities of bacterioplankton (Figure 6; Points), the spheres of lowered local $[H_2O_2]$ would overlap when $[H_2O_2]$ intracellular:extracellular ratio is less than or equal to 0.01 (Figure 6, short dashed line). However, the limited available information [58] suggests that heterotrophic bacteria maintain an $[H_2O_2]$ intracellular:extracellular ratio of about 0.1 (Figure 6, dotted line). It is possible that cells may not be able to maintain an intracellular:extracellular $[H_2O_2]$ ratio of 0.1 at the lowest seawater $[H_2O_2]$ given the likely roles of H_2O_2 in cell signaling [36], and the need to maintain a basal $[H_2O_2]$ [44]. The authors of [58] predict an intracellular steady-state $[H_2O_2]$ of 20 nM in heterotrophs in the absence of extracellular H_2O_2, which would suggest that at low extracellular $[H_2O_2]$, the intracellular:extracellular $[H_2O_2]$ ratio would be >0.1, and the spheres of lowered local $[H_2O_2]$ would not overlap (Figure 6). Thus, the cell-specific effects of bacterioplankton upon local $[H_2O_2]$ are unlikely to overlap at reasonable cell suspension densities.

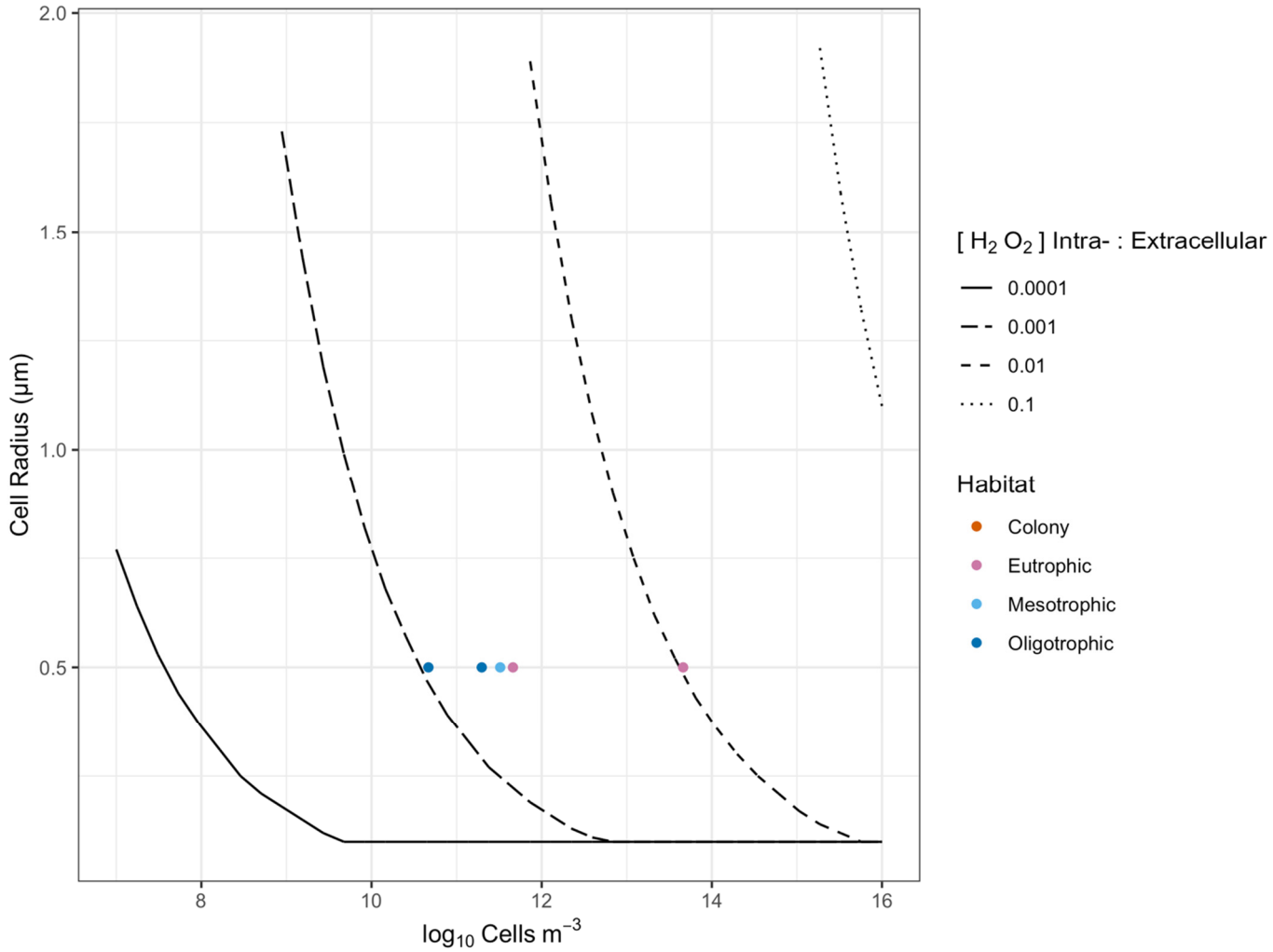

Figure 6. Thresholds for direct bacterioplankton cell-to-cell interaction through $[H_2O_2]$ above seawater background. The X axis shows a range of cell m^{-3} (which in turn governs cell-to-cell distances), while the Y axis shows radii for cell-specific spheres of influence upon $[H_2O_2]$ (a function of cell size, intracellular $[H_2O_2]$ and seawater $[H_2O_2]$). The areas below the threshold lines show combinations where bacterioplankton cell-to-cell distance exceeds the cell-specific $[H_2O_2]$ distance, so direct cell-to-cell interactions mediated by $[H_2O_2]$ are unlikely. The area above the threshold lines show combinations where bacterioplankton cell-to-cell distance is less than the cell-specific $[H_2O_2]$ distance, so direct cell-to-cell interactions mediated by $[H_2O_2]$ are feasible. The four threshold lines refer to a range of ratios of bacterioplankton intracellular to extracellular $[H_2O_2]$. Data points from different habitats show that direct bacterioplankton cell-to-cell interactions are likely, over a range of reasonable ratios of intracellular to extracellular $[H_2O_2]$, at $>10^{10}$ cells m^{-3}.

3. Conclusions

Our approximations of cell-to-cell spacing are applied to each taxa x habitat combination separately, based upon published measures of cell suspension densities in marine systems. We then overlaid the taxa-specific simulations from a given habitat to give a visualization of community level cell-to-cell spacings, across taxa within a habitat (Figure 1). As a next step we aim to implement probability distributions of cell-to-cell spacings across all cells from a mixed community in the habitat, to more accurately capture the likelihood of cell-to-cell interactions. Our work used available cell suspension density data exclusively from marine habitats. In general, we would assume that if cell densities and $[H_2O_2]$ in freshwater systems are similar to that of marine systems, the diffusional patterns described

for marine habitats would be comparable to freshwater systems, but future studies would need to confirm this.

Our simple approximations of diffusion gradients out from cells are limited by a dearth of published information on the intracellular concentrations of H_2O_2, and other ROS, in phytoplankton or bacterioplankton cells. There are published estimates of intracellular and extracellular H_2O_2 production and decay rates in seawater, which could support more sophisticated reaction/diffusion simulation approaches.

The threshold lines for interacting cell-specific spheres of influence as functions of cell radii and cell suspension densities are generated for individual 'taxa' from marine environments with uniform intracellular [H_2O_2] (Figure 5), rather than for a mixed community of different cell sizes and physiologies. These fixed threshold lines also apply to a fixed ratio of internal to external [H_2O_2], whereas this ratio could vary rapidly with changes in cell physiology and external conditions, causing the threshold for direct cell-to-cell interactions to shift. Our models suggest that it is unlikely that H_2O_2 diffusing out of a phytoplankton cell directly interacts with another phytoplankton cell at natural seawater cell densities (Figure 5), with the exception of *Phaeocystis*, whereby H_2O_2 diffusing out of a cell would directly interact with other cells if the intracellular:extracellular [H_2O_2] ratio is greater than 100. A future approach aims to generate probability distributions for direct cell-to-cell interactions, since even populations with widely spaced cells occasionally generate close cell-to-cell distances. Analyses show higher rates of cell-normalized H_2O_2 production in bloom-forming phytoplankton taxa, providing support for the selective influence of cell suspension density upon ROS dynamics [29].

It is likely that extracellular ROS play a role in the growth and development of phytoplankton, given that [74] found that the addition of superoxide dismutase and catalase inhibited the growth of *Chattonella marina*. Our models suggest that H_2O_2 diffusing out of phytoplankton cells reaches external [H_2O_2] before interacting with other cells (Figures 3 and 5), and are primarily driven by the influence of diffusion, and with negligible contribution from the decay of H_2O_2 (Figure 2). Indirect interaction of H_2O_2 diffusing out of cells is also possible as H_2O_2 can affect biogeochemical cycles and bioavailability of nutrients [75].

The simple estimates presented herein using H_2O_2 as a case study are generalizable to other, less stable ROS where decay will be a more immediate influence. For example, $O_2^{\bullet-}$ itself is not cell membrane permeable and so forms separate intra- and extracellular pools. However, $O_2^{\bullet-}$ is metabolized to H_2O_2, both inside and outside cells, and so could indirectly influence [H_2O_2], and thereby alter cell-to-cell interactions beyond the simple diffusion-dominated simulations we present. For example, extracellular production of $O_2^{\bullet-}$ by heterotrophic bacteria can significantly alter $O_2^{\bullet-}$ concentrations in the dark ocean [28]. Heterotrophs might also produce enough $O_2^{\bullet-}$ to indirectly influence concentrations of $O_2^{\bullet-}$ in the photic zone of the ocean. The phytoplankter *T. weissflogii* [34] generates ranges of ~8×10^{-16} mol $O_2^{\bullet-}$ cell^{-1} hr^{-1}, while four raphidophytes show production ranges of 0.45 to 4×10^{-12} mol $O_2^{\bullet-}$ cell^{-1} hr^{-1} [76], illustrating the wide range of extracellular production which can differentially influence extracellular [ROS] across communities or conditions.

The approaches presented here are a step towards visualizing and constraining estimates of cell-to-cell interactions in plankton communities. We next need to validate these approaches with quantitative estimates of intracellular [H_2O_2], and other [ROS], within phytoplankton and bacterioplankton cells.

4. Methods, Simplifying Assumptions, and Limitations

4.1. Estimation of Cell to Cell Spacing

A simplistic estimator of cell-to-cell spacing is the reciprocal of the cube root of the cell suspension density. For example, if cell suspension density is expressed as cells μL^{-1} (equivalent to cells mm^{-3}), the reciprocal of the cube root gives a cell-to-cell spacing estimate in mm. This cube root estimate assumes equally spaced cells, which somewhat

overestimates average cell-to-cell spacing, since equally spaced cells give a maximum spacing, not the average spacing of randomly located cells. An arithmetic correction based upon the gamma function of 4/3 generates a numeric correction to multiply the reciprocal of the cube root of the cell suspension density by 0.55 to approximate average spacing of cells [77] (Equation (2)).

$$CellSpace\ \text{mm} = \sqrt[3]{\frac{1}{Cell\ Count\ \mu\text{L}^{-1}}} * 0.55 \quad (2)$$

We generated simulated cell suspension densities for each taxa and habitat by generating points separated by the average cell spacing between cells, along each of the X, Y, Z spatial axes. We then added random variation to the values of the evenly spaced points (R jitter, factor = 2), to generate a XYZ coordinate cloud. In a parallel approach (data not presented) we directly generated normally distributed random distributions around the average cell spacings, but that approach was computationally slow for denser cell suspension densities. Overlaying the results from co-occurring taxa then gives a visualization of the community in a habitat (Figure 1). Although overlaying data from separately simulated taxa is adequate for visualization, a more sophisticated model would be required to explicitly generate and retrieve the distributions of cell-to-cell distances within, or across, taxa. Furthermore, even in oligotrophic habitats with low average cell suspension densities the few cells present may be clustered non-randomly, an ecological nuance not captured in our approach.

4.2. Simulating Concentration Gradients

To simulate H_2O_2 concentration gradients generated around a given cell, we consider the cell as a fixed spherical volume which maintains a steady, homeostatic intracellular [H_2O_2]. For simulation of phytoplankton cells, we set a homeostatic intracellular [H_2O_2] of 10^{-6} M, based upon limited literature from other eukaryotes [61], and as a level below the cytotoxic threshold of 10^{-5} M. For simulation of bacterioplankton cells, we set a homeostatic intracellular [H_2O_2] of 1/10 the external seawater [H_2O_2] [58,60].

Using the H_2O_2 diffusion co-efficient in water, and time increments from 0 µs with a $\log_{10}$ series upwards to 100 µs, we calculate the progressive net diffusional displacement of H_2O_2 outward from the cell surface. We then estimate dilution of [H_2O_2] with diffusion outwards from a source 'Phytoplankton' cell or diffusion inwards towards a sink 'Heterotrophic' cell. In addition to the simple volumetric dilution as ROS diffuses outwards from 'Phytoplankton' cells, we add a time-dependent decay term based upon measured lifetimes of H_2O_2 in seawater, which also vary widely. We use nominal time increments to generate the diffusion distances of H_2O_2 outward from the cell and to simulate the concurrent effect of pseudo-first order decay as H_2O_2 moves outward from the cell with time, but this simple simulation assumes a steady state, without considering local mixing or fluctuations in cellular or environmental H_2O_2.

4.3. Simulating Threshold Radii for [H_2O_2] above or below Seawater [H_2O_2]

On a visual plot, the intersect of the [H_2O_2] outwards from a 'Phytoplankton' source cell, with the lowest seawater [H_2O_2] is obvious, but it proved challenging to estimate this threshold distance when outwardly diffusing [H_2O_2] declines to the lowest seawater [H_2O_2]. The time for [H_2O_2] to decline to seawater [H_2O_2] depends upon the ratio of intracellular:extracellular [H_2O_2]; the diffusion coefficient for ROS, which determines how far [H_2O_2] moves out from the cell radius in a given time interval; and thus the [H_2O_2] volumetric dilution factor over a given time interval. For [H_2O_2], concomitant decay was only a negligible factor, but to retain capacity for generalizations to other, less stable [ROS] we nevertheless included an extracellular decay rate constant in the estimations. After algebraic transforms we found that a LambertW function was appropriate [78] to estimate

the threshold radius at which $[H_2O_2]$ around a cell falls to the lowest seawater $[H_2O_2]$ (Equation (3)).

In Equation (3), $[H_2O_2]_{seawater}$ is the seawater $[H_2O_2]$ in the simulated habitat in mol L^{-1}; $[H_2O_2]_{cell}$ is the intracellular homeostatic $[H_2O_2]$ in mol L^{-1}; $DiffusionRad_{threshold}$ in μm is the radius of the diffusion sphere when $[H_2O_2]$ drops to $[H_2O_2]_{seawater}$; CellRadius is the radius of the cell in μm; μ is the pseudo-first order decay constant for H_2O_2 in seawater; $us_{threshold}$ is the time in μs at which $[H_2O_2]$ drops to $[H_2O_2]_{seawater}$; Diffusion Coefficient (D) is expressed in $\mu m^2\ \mu s^{-1}$; W_0 is the Lambert W function, also known as the Omega function, used to solve for $f(x) = xe^x$.

$$
\begin{aligned}
[H_2O_2]_{seawater} &= [H_2O_2]_{cell} * \frac{\frac{4}{3}*\pi*(CellRadius)^3}{\frac{4}{3}*\pi*DiffusionRad_{threshold}^3} * e^{-\mu*us_{threshold}} \\
[H_2O_2]_{seawater} &= [H_2O_2]_{cell} * \frac{(CellRadius)^3}{DiffusionRad_{threshold}^3} * e^{-\mu*us_{threshold}} \\
[H_2O_2]_{seawater} &= [H_2O_2]_{cell} * \frac{(CellRadius)^3}{\left(CellRadius + \sqrt[2]{D*us_{threshold}}\right)^3} * e^{-\mu*us_{threshold}} \\
\frac{[H_2O_2]_{seawater}}{[H_2O_2]_{cell}*(CellRadius)^3} &= \frac{1}{\left(CellRadius + \sqrt[2]{D*us_{threshold}}\right)^3} * e^{-\mu*us_{threshold}} \\
\frac{[H_2O_2]_{seawater}}{[H_2O_2]_{cell}*(CellRadius)^3} &= k \\
\sqrt[3]{k} &= \frac{1}{\left(CellRadius + \sqrt[2]{D*us_{threshold}}\right)} * e^{\frac{-\mu*us_{threshold}}{3}} \\
CellRadius + \sqrt[2]{D*us_{threshold}} &= \frac{e^{\frac{-\mu*us_{threshold}}{3}}}{\sqrt[3]{k}} \\
\sqrt[2]{D*us_{threshold}} &= \frac{e^{\frac{-\mu*us_{threshold}}{3}}}{\sqrt[3]{k}} - CellRadius \\
\frac{\sqrt[2]{D*us_{threshold}}}{e^{\frac{-\mu*us_{threshold}}{3}}} &= \frac{1}{\sqrt[3]{k}} - CellRadius \\
\frac{D*us_{threshold}}{e^{\frac{-\mu*us_{threshold}*2}{3}}} &= \left(\frac{1}{\sqrt[3]{k}} - CellRadius\right)^2 \\
D*us_{threshold}*e^{\frac{\mu*us_{threshold}*2}{3}} &= \left(\frac{1}{\sqrt[3]{k}} - CellRadius\right)^2 \\
us_{threshold}*e^{\frac{\mu*us_{threshold}*2}{3}} &= \frac{\left(\frac{1}{\sqrt[3]{k}} - CellRadius\right)^2}{D} \\
\frac{\mu*us_{threshold}*2}{3} &= Y \\
\frac{Y}{\mu*\frac{2}{3}}*e^Y &= \frac{\left(\frac{1}{\sqrt[3]{k}} - CellRadius\right)^2}{D} \\
Y*e^Y &= \frac{\left(\frac{1}{\sqrt[3]{k}} - CellRadius\right)^2}{D} * \mu * \frac{2}{3} \\
Y &= W_0\left(\frac{\left(\frac{1}{\sqrt[3]{\frac{[H_2O_2]_{seawater}}{[H_2O_2]_{cell}*(CellRadius)^3}}} - CellRadius\right)^2}{D} * \mu * \frac{2}{3}\right) \\
us_{threshold} &= \frac{W_0\left(\frac{\left(\frac{1}{\sqrt[3]{\frac{[H_2O_2]_{seawater}}{[H_2O_2]_{cell}*(CellRadius)^3}}} - CellRadius\right)^2}{D} * \mu * \frac{2}{3}\right)}{\left(\mu * \frac{2}{3}\right)}
\end{aligned}
\tag{3}
$$

For 'Heterotrophic' sink cells we simulated the sphere of $[H_2O_2]$ below seawater $[H_2O_2]$ accounting only for diffusion around the cell without including a rate constant for time-dependent bulk decay because the cell is acting, on top of any decay term, to further lower $[H_2O_2]$ below seawater $[H_2O_2]$ (Reaction (4)).

$$[H_2O_2]_{seawater} = [H_2O_2]_{cell} * \left(DiffusionSphere_{threshold}\right) / ((4/3) * \pi * CellRadius)$$

where $[H_2O_2]_{seawater}$ is again the seawater $[H_2O_2]$ in the simulated habitat in mol L^{-1}; $[H_2O_2]_{cell}$ is the intracellular homeostatic $[H_2O_2]$ in mol L^{-1}; and $DiffusionRad_{threshold}$ in µm is the radius of the diffusion sphere when $[H_2O_2]$ drops to $[H_2O_2]_{seawater}$; CellRadius is the radius of the cell in µm.

Alter substitutions and re-arrangements:

Where µs_thresh is the elapsed time in µs to reach the threshold $[H_2O_2]$; Diffusion Coefficient (D) is expressed in $\mu m^2\ \mu s^{-1}$; µs [1] is the first simulated time step. We then recover the threshold distance as:

$$\begin{aligned} [H_2O_2]_{seawater} &= [H_2O_2]_{cell} * \frac{(4/3)*\pi*DiffusionRad_{threshold}^3}{(4/3)*\pi*CellRadius^3} \\ [H_2O_2]_{seawater} &= [H_2O_2]_{cell} * \frac{DiffuseRad_{threshold}^3}{CellRadius^3} \\ \frac{[H_2O_2]_{seawater}}{[H_2O_2]_{cell}} &= \left(\frac{DiffuseRad_{threshold}}{CellRadius}\right)^3 \\ DiffuseRad_{threshold} &= \sqrt[3]{\frac{[H_2O_2]_{seawater}}{[H_2O_2]_{cell}}} * CellRadius \end{aligned} \quad (4)$$

4.4. Simulations and Plotting

We used R [79] running under RStudio [80], using packages 'tidyverse' [81], 'pracma' [82], 'ggplot2' [83], 'cowplot' [84], 'ggpubr' [85], 'glue' [86], 'kableExtra' [87], 'LambertW' [88], 'ggforce' [89], 'googledrive' [90], and 'googlesheets4' [91]. Citations were managed using Zotero [92] open access reference manager connected to RStudio using the 'citr' [93] package, with output generated using the 'knitr' [94–96] and 'bookdown' [97] packages.

Author Contributions: N.M.O. assembled the relevant literature, helped generate the mathematical formulations and figures and contributed to writing and completing the manuscript draft. O.P. contributed to the generation of the initial ideas and contributed to the manuscript draft. J.S.P.M. contributed ideas, literature and in particular formulated the concept for Figure 5. D.A.C. contributed to the generation of initial ideas, wrote the manuscript draft and helped complete the manuscript. All authors contributed extensive revisions and edits to the manuscript. All authors have read and agreed to the published version of the manuscript.

Funding: NMO was supported by the Mount Allison University Rice Memorial Graduate Fellowship and a New Brunswick Innovation Foundation STEM Graduate Award. DAC was supported by the Canada Research Chair in Phytoplankton Ecophysiology and by the Microbiology Institute of the Czech Academy of Science through project CZ.02.2.69/0.0/0.0/16_027/0007990 of the European Union Researcher Mobility program.

Institutional Review Board Statement: Not applicable.

Informed Consent Statement: Not applicable.

Data Availability Statement: The RStudio workbook used to generate this document is hosted at https://github.com/NaamanOmar/ROS_bioinfo.git.

Acknowledgments: The authors thank Maximilian Berthold for his comments.

Conflicts of Interest: The authors declare no conflict of interest.

References

1. Reynolds, C.S. *The Ecology of Phytoplankton*; Cambridge University Press: Cambridge, UK, 2006; ISBN 978-1-139-45489-6.
2. Falkowski, P.G.; Katz, M.E.; Knoll, A.H.; Quigg, A.; Raven, J.A.; Schofield, O.; Taylor, F.J.R. The Evolution of Modern Eukaryotic Phytoplankton. *Sci. Wash.* **2004**, *305*, 354–360. [CrossRef] [PubMed]

3. Purcell, E.M. Life at Low Reynolds Number. *Am. J. Phys.* **1976**, *45*, 3–11. [CrossRef]
4. Finkel, Z.V.; Beardall, J.; Flynn, K.J.; Quigg, A.; Rees, T.A.V.; Raven, J.A. Phytoplankton in a Changing World: Cell Size and Elemental Stoichiometry. *J. Plankton Res.* **2010**, *32*, 119–137. [CrossRef]
5. Stolte, W.; Riegman, R. Effect of Phytoplankton Cell Size on Transient-State Nitrate and Ammonium Uptake Kinetics. *Microbiology* **1995**, *141*, 1221–1229. [CrossRef] [PubMed]
6. Gemmell, B.J.; Oh, G.; Buskey, E.J.; Villareal, T.A. Dynamic Sinking Behaviour in Marine Phytoplankton: Rapid Changes in Buoyancy May Aid in Nutrient Uptake. *Proc. R. Soc. B Biol. Sci.* **2016**, *283*, 20161126. [CrossRef]
7. Bertrand, E.M.; McCrow, J.P.; Moustafa, A.; Zheng, H.; McQuaid, J.B.; Delmont, T.O.; Post, A.F.; Sipler, R.E.; Spackeen, J.L.; Xu, K.; et al. Phytoplanktonbacterial Interactions Mediate Micronutrient Colimitation at the Coastal Antarctic Sea Ice Edge. *Proc. Natl. Acad. Sci. USA* **2015**, *112*, 9938–9943. [CrossRef]
8. Jakobsen, H.; Tang, K. Effects of Protozoan Grazing on Colony Formation in *Phaeocystis Globosa* (Prymnesiophyceae) and the Potential Costs and Benefits. *Aquat. Microb. Ecol.* **2002**, *27*, 261–273. [CrossRef]
9. Robarts, R.; Zohary, T.; Waiser, M.; Yacobi, Y. Bacterial Abundance, Biomass, and Production in Relation to Phytoplankton Biomass in the Levantine Basin of the Southeastern Mediterranean Sea. *Mar. Ecol. Prog. Ser.* **1996**, *137*, 273–281. [CrossRef]
10. Grob, C.; Ulloa, O.; Li, W.; Alarcón, G.; Fukasawa, M.; Watanabe, S. Picoplankton Abundance and Biomass Across the Eastern South Pacific Ocean Along Latitude 32.5. *Mar. Ecol. Prog. Ser.* **2007**, *332*, 53–62. [CrossRef]
11. Olguín, H.F.; Boltovskoy, D.; Lange, C.B.; Brandini, F.; Flynn, K.J. Distribution of Spring Phytoplankton (Mainly Diatoms) in the Upper 50 m of the Southwestern Atlantic Ocean (30). *J. Plankton Res.* **2006**, *28*, 1107–1128. [CrossRef]
12. Agustí, S.; Llabrés, M. Solar Radiation-induced Mortality of Marine Pico-phytoplankton in the Oligotrophic Ocean. *Photochem. Photobiol.* **2007**, *83*, 793–801. [CrossRef] [PubMed]
13. Klinkenberg, G.; Schumann, R. Abundance Changes of Autotrophic and Heterotrophic Picoplankton in the Zingster Strom, a Shallow, Tideless Estuary South of the Darß-Zingst Peninsula (Southern Baltic Sea). *Arch. Hydrobiol.* **1995**, *134*, 359–377. [CrossRef]
14. Albrecht, M.; Pröschold, T.; Schumann, R. Identification of Cyanobacteria in a Eutrophic Coastal Lagoon on the Southern Baltic Coast. *Front. Microbiol.* **2017**, *8*, 923. [CrossRef] [PubMed]
15. Pintoa, E.; Van Nieuwerburgha, L.; De Barros, M.P.; Pedersén, M.; Colepicolo, P.; Snoeijs, P. Density-Dependent Patterns of Thiamine and Pigment Production in the Diatom *Nitzschia Microcephala*. *Phytochemistry* **2003**, *63*, 155–163. [CrossRef]
16. Fogel, M.L.; Cifuentes, L.A.; Velinsky, D.J.; Sharp, J.H. Relationship of Carbon Availability in Estuarine Phytoplankton to Isotopic Composition. *Mar. Ecol. Prog. Ser.* **1992**, *82*, 291–301. [CrossRef]
17. Hansen, P.J.; Lundholm, N.; Rost, B. Growth Limitation in Marine Red-Tide Dinoflagellates: Efects of pH Versus Inorganic Carbon Availability. *Mar. Ecol. Prog. Ser.* **2007**, *334*, 10. [CrossRef]
18. Avery, G.B.; Cooper, W.J.; Kieber, R.J.; Willey, J.D. Hydrogen Peroxide at the Bermuda Atlantic Time Series Station: Temporal Variability of Seawater Hydrogen Peroxide. *Mar. Chem.* **2005**, *97*, 236–244. [CrossRef]
19. Kearns, K.D.; Hunter, M.D. Algal Extracellular Products Suppress Anabaena Flos-Aquae Heterocyst Spacing. *Microb. Ecol.* **2002**, *43*, 174–180. [CrossRef]
20. Biller, S.J.; Berube, P.M.; Lindell, D.; Chisholm, S.W. *Prochlorococcus*: The Structure and Function of Collective Diversity. *Nat. Rev. Microbiol.* **2015**, *13*, 13–27. [CrossRef]
21. Kozuleva, M.A.; Ivanov, B.N.; Vetoshkina, D.V.; Borisova-Mubarakshina, M.M. Minimizing an Electron Flow to Molecular Oxygen in Photosynthetic Electron Transfer Chain: An Evolutionary View. *Front. Plant Sci.* **2020**, *11*, 211. [CrossRef]
22. Sharma, P.; Jha, A.B.; Dubey, R.S.; Pessarakli, M. Reactive Oxygen Species, Oxidative Damage, and Antioxidative Defense Mechanism in Plants Under Stressful Conditions. *J. Bot.* **2012**, *2012*, e217037. [CrossRef]
23. Li, R.; Jia, Z.; Trush, M.A. Defining ROS in Biology and Medicine. *React. Oxyg. Species (Apex)* **2016**, *1*, 9–21. [CrossRef] [PubMed]
24. Radi, R. Oxygen Radicals, Nitric Oxide, and Peroxynitrite: Redox Pathways in Molecular Medicine. *Proc. Natl. Acad. Sci. USA* **2018**, *115*, 5839–5848. [CrossRef]
25. Fridovich, I. Oxygen Toxicity: A Radical Explanation. *J. Exp. Biol.* **1998**, *201*, 1203–1209. [CrossRef]
26. Zinser, E.R. The Microbial Contribution to Reactive Oxygen Species Dynamics in Marine Ecosystems. *Environ. Microbiol. Rep.* **2018**, *10*, 412–427. [CrossRef] [PubMed]
27. Zhang, T.; Hansel, C.M.; Voelker, B.M.; Lamborg, C.H. Extensive Dark Biological Production of Reactive Oxygen Species in Brackish and Freshwater Ponds. *Environ. Sci. Technol.* **2016**, *50*, 2983–2993. [CrossRef] [PubMed]
28. Diaz, J.M.; Hansel, C.M.; Voelker, B.M.; Mendes, C.M.; Andeer, P.F.; Zhang, T. Widespread Production of Extracellular Superoxide by Heterotrophic Bacteria. *Science* **2013**, *340*, 1223–1226. [CrossRef] [PubMed]
29. Diaz, J.M.; Plummer, S. Production of Extracellular Reactive Oxygen Species by Phytoplankton: Past and Future Directions. *J. Plankton Res.* **2018**, *40*, 655–666. [CrossRef]
30. Diaz, J.M.; Plummer, S.; Tomas, C.; Alves-de-Souza, C. Production of Extracellular Superoxide and Hydrogen Peroxide by Five Marine Species of Harmful Bloom-Forming Algae. *J. Plankton Res.* **2018**, *40*, 667–677. [CrossRef]
31. Rose, A.L.; Webb, E.A.; Waite, T.D.; Moffett, J.W. Measurement and Implications of Nonphotochemically Generated Superoxide in the Equatorial Pacific Ocean. *Environ. Sci. Technol.* **2008**, *42*, 2387–2393. [CrossRef]
32. Schneider, R.J.; Roe, K.L.; Hansel, C.M.; Voelker, B.M. Species-Level Variability in Extracellular Production Rates of Reactive Oxygen Species by Diatoms. *Front. Chem.* **2016**, *4*, 5. [CrossRef] [PubMed]

33. Sutherland, K.M.; Coe, A.; Gast, R.J.; Plummer, S.; Suffridge, C.P.; Diaz, J.M.; Bowman, J.S.; Wankel, S.D.; Hansel, C.M. Extracellular Superoxide Production by Key Microbes in the Global Ocean. *Limnol. Oceanogr.* **2019**, *64*, 2679–2693. [CrossRef]
34. Kustka, A.B.; Shaked, Y.; Milligan, A.J.; King, D.W.; Morel, F.M.M. Extracellular Production of Superoxide by Marine Diatoms: Contrasting Effects on Iron Redox Chemistry and Bioavailability. *Limnol. Oceanogr.* **2005**, *50*, 1172–1180. [CrossRef]
35. Hansel, C.M.; Buchwald, C.; Diaz, J.M.; Ossolinski, J.E.; Dyhrman, S.T.; Mooy, B.A.S.V.; Polyviou, D. Dynamics of Extracellular Superoxide Production by Trichodesmium Colonies from the Sargasso Sea. *Limnol. Oceanogr.* **2016**, *61*, 1188–1200. [CrossRef]
36. Mittler, R.; Vanderauwera, S.; Suzuki, N.; Miller, G.; Tognetti, V.B.; Vandepoele, K.; Gollery, M.; Shulaev, V.; Breusegem, F.V. ROS Signaling: The New Wave? *Trends Plant Sci.* **2011**, *16*, 300–309. [CrossRef]
37. Rhee, S.G. H_2O_2, a Necessary Evil for Cell Signaling. *Science* **2006**, *312*, 1882–1883. [CrossRef]
38. del Río, L.A.; López-Huertas, E. ROS Generation in Peroxisomes and Its Role in Cell Signaling. *Plant Cell Physiol.* **2016**, *57*, 1364–1376. [CrossRef]
39. del Río, L.A.; Puppo, A. (Eds.) *Reactive Oxygen Species in Plant Signaling, Signaling and Communication in Plants*; Springer: Dordrecht, The Netherlands; New York, NY, USA, 2009; ISBN 978-3-642-00389-9/978-3-642-00390-5.
40. Foyer, C.H.; Noctor, G. Redox Homeostasis and Antioxidant Signaling: A Metabolic Interface Between Stress Perception and Physiological Responses. *Plant Cell* **2005**, *17*, 1866–1875. [CrossRef]
41. Schmitt, F.-J.; Renger, G.; Friedrich, T.; Kreslavski, V.D.; Zharmukhamedov, S.K.; Los, D.A.; Kuznetsov, V.V.; Allakhverdiev, S.I. Reactive Oxygen Species: Re-evaluation of Generation, Monitoring and Role in Stress-Signaling in Phototrophic Organisms. *Biochim. Biophys. Acta (BBA) Bioenerg.* **2014**, *1837*, 835–848. [CrossRef]
42. Miller, G.; Suzuki, N.; Ciftci-Yilmaz, S.; Mittler, R. Reactive Oxygen Species Homeostasis and Signalling During Drought and Salinity Stresses. *Plant Cell Environ.* **2010**, *33*, 453–467. [CrossRef]
43. Shi, K.; Gao, Z.; Shi, T.-Q.; Song, P.; Ren, L.-J.; Huang, H.; Ji, X.-J. Reactive Oxygen Species-Mediated Cellular Stress Response and Lipid Accumulation in Oleaginous Microorganisms: The State of the Art and Future Perspectives. *Front. Microbiol.* **2017**, *8*, 793. [CrossRef] [PubMed]
44. Mittler, R. ROS Are Good. *Trends Plant Sci.* **2017**, *22*, 11–19. [CrossRef] [PubMed]
45. Schneider, R. Kinetics of Biological Hydrogen Peroxide Production. Ph.D. Thesis, Colorado School of Mines, Golden, CO, USA, 2015.
46. Millero, F.J.; Sharma, V.K.; Karn, B. The Rate of Reduction of Copper(II) with Hydrogen Peroxide in Seawater. *Mar. Chem.* **1991**, *36*, 71–83. [CrossRef]
47. Moffett, J.W.; Zika, R.G. Reaction Kinetics of Hydrogen Peroxide with Copper and Iron in Seawater. *Environ. Sci. Technol.* **1987**, *21*, 804–810. [CrossRef] [PubMed]
48. Kelly, T.J.; Daum, P.H.; Schwartz, S.E. Measurements of Peroxides in Cloudwater and Rain. *J. Geophys. Res. Atmos.* **1985**, *90*, 7861–7871. [CrossRef]
49. Morris, J.J.; Johnson, Z.I.; Wilhelm, S.W.; Zinser, E.R. Diel Regulation of Hydrogen Peroxide Defenses by Open Ocean Microbial Communities. *J. Plankton Res.* **2016**, *38*, 1103–1114. [CrossRef]
50. Yuan, J.; Shiller, A.M. The Distribution of Hydrogen Peroxide in the Southern and Central Atlantic Ocean. *Deep Sea Res. Part II Top. Stud. Oceanogr.* **2001**, *48*, 2947–2970. [CrossRef]
51. Tjell, A.Ø.; Almdal, K. Diffusion Rate of Hydrogen Peroxide Through Water-Swelled Polyurethane Membranes. *Sens. Bio-Sens. Res.* **2018**, *21*, 35–39. [CrossRef]
52. Lesser, M.P. Oxidative Stress in Marine Environments: Biochemistry and Physiological Ecology. *Annu. Rev. Physiol.* **2006**, *68*, 253–278. [CrossRef]
53. Halliwell, B.; Gutteridge, J.M.C. *Free Radicals in Biology and Medicine*, 3rd ed.; Oxford Science Publications: Oxford, UK; Clarendon Press, Oxford University Press: Oxford, UK, 1999; ISBN 978-0-19-850045-2/978-0-19-850044-5.
54. González-Flecha, B.; Demple, B. Homeostatic Regulation of Intracellular Hydrogen Peroxide Concentration in Aerobically Growing Escherichia Coli. *J. Bacteriol.* **1997**, *179*, 382–388. [CrossRef]
55. Lyublinskaya, O.; Antunes, F. Measuring Intracellular Concentration of Hydrogen Peroxide with the Use of Genetically Encoded H_2O_2 Biosensor HyPer. *Redox Biol.* **2019**, *24*, 101200. [CrossRef] [PubMed]
56. Stone, J.R.; Yang, S. Hydrogen Peroxide: A Signaling Messenger. *Antioxid. Redox Signal.* **2006**, *8*, 243–270. [CrossRef] [PubMed]
57. Sies, H. Hydrogen Peroxide as a Central Redox Signaling Molecule in Physiological Oxidative Stress: Oxidative Eustress. *Redox Biol.* **2017**, *11*, 613–619. [CrossRef]
58. Seaver, L.C.; Imlay, J.A. Hydrogen Peroxide Fluxes and Compartmentalization Inside Growing *Escherichia Coli*. *J. Bacteriol.* **2001**, *183*, 7182–7189. [CrossRef] [PubMed]
59. Huang, B.K.; Sikes, H.D. Quantifying Intracellular Hydrogen Peroxide Perturbations in Terms of Concentration. *Redox Biol.* **2014**, *2*, 955–962. [CrossRef]
60. Li, X.; Imlay, J.A. Improved Measurements of Scant Hydrogen Peroxide Enable Experiments That Define Its Threshold of Toxicity for *Escherichia Coli*. *Free Radic. Biol. Med.* **2018**, *120*, 217–227. [CrossRef]
61. Forman, H.J.; Bernardo, A.; Davies, K.J.A. What Is the Concentration of Hydrogen Peroxide in Blood and Plasma? *Arch. Biochem. Biophys.* **2016**, *603*, 48–53. [CrossRef]
62. Winterbourn, C.C.; Hampton, M.B. Thiol Chemistry and Specificity in Redox Signaling. *Free Radic. Biol. Med.* **2008**, *45*, 549–561. [CrossRef]

63. Apel, K.; Hirt, H. Reactive Oxygen Species: Metabolism, Oxidative Stress, and Signal Transduction. *Annu. Rev. Plant Biol.* **2004**, *55*, 373–399. [CrossRef]
64. Fedurayev, P.V.; Mironov, K.S.; Gabrielyan, D.A.; Bedbenov, V.S.; Zorina, A.A.; Shumskaya, M.; Los, D.A. Hydrogen Peroxide Participates in Perception and Transduction of Cold Stress Signal in Synechocystis. *Plant Cell Physiol.* **2018**, *59*, 1255–1264. [CrossRef]
65. Khademian, M.; Imlay, J.A. *Escherichia Coli* Cytochrome c Peroxidase Is a Respiratory Oxidase That Enables the Use of Hydrogen Peroxide as a Terminal Electron Acceptor. *Proc. Natl. Acad. Sci. USA* **2017**, *114*, E6922–E6931. [CrossRef] [PubMed]
66. Bienert, G.P.; Chaumont, F. Aquaporin-Facilitated Transmembrane Diffusion of Hydrogen Peroxide. *Biochim. Biophys. Acta* **2014**, *1840*, 1596–1604. [CrossRef] [PubMed]
67. Almasalmeh, A.; Krenc, D.; Wu, B.; Beitz, E. Structural Determinants of the Hydrogen Peroxide Permeability of Aquaporins. *FEBS J.* **2014**, *281*, 647–656. [CrossRef] [PubMed]
68. Wang, H.; Schoebel, S.; Schmitz, F.; Dong, H.; Hedfalk, K. Characterization of Aquaporin-Driven Hydrogen Peroxide Transport. *Biochim. Biophys. Acta (BBA) Biomembr.* **2020**, *1862*, 183065. [CrossRef]
69. Miller, E.W.; Dickinson, B.C.; Chang, C.J. Aquaporin-3 Mediates Hydrogen Peroxide Uptake to Regulate Downstream Intracellular Signaling. *Proc. Natl. Acad. Sci. USA* **2010**, *107*, 15681–15686. [CrossRef]
70. Bond, R.J.; Hansel, C.M.; Voelker, B.M. Heterotrophic Bacteria Exhibit a Wide Range of Rates of Extracellular Production and Decay of Hydrogen Peroxide. *Front. Mar. Sci.* **2020**, *7*, 72. [CrossRef]
71. Coe, A.; Ghizzoni, J.; LeGault, K.; Biller, S.; Roggensack, S.E.; Chisholm, S.W. Survival of Prochlorococcus in Extended Darkness. *Limnol. Oceanogr.* **2016**, *61*, 1375–1388. [CrossRef]
72. Zinser, E.R. Cross-Protection from Hydrogen Peroxide by Helper Microbes: The Impacts on the Cyanobacterium *Prochlorococcus* and Other Beneficiaries in Marine Communities. *Environ. Microbiol. Rep.* **2018**, *10*, 199–411. [CrossRef]
73. Zhu, Z.; Meng, R.; Smith, W.O., Jr.; Doan-Nhu, H.; Nguyen-Ngoc, L.; Jiang, X. Bacterial Composition Associated With Giant Colonies of the Harmful Algal Species Phaeocystis Globosa. *Front. Microbiol.* **2021**, *12*, 737484. [CrossRef]
74. Oda, T.; Moritomi, J.; Kawano, I.; Hamaguchi, S.; Ishimatsu, A.; Muramatsu, T. Catalase- and Superoxide Dismutase-induced Morphological Changes and Growth Inhibition in the Red Tide Phytoplankton *Chattonella Marina*. *Biosci. Biotechnol. Biochem.* **1995**, *59*, 2044–2048. [CrossRef]
75. Morris, J.J.; Rose, A.L.; Lu, Z. Reactive Oxygen Species in the World Ocean and Their Impacts on Marine Ecosystems. *Redox Biol.* **2022**, *52*, 102285. [CrossRef] [PubMed]
76. Oda, T.; Nakamura, A.; Shikayama, M.; Kawano, I.; Ishimatsu, A.; Muramatsu, T. Generation of Reactive Oxygen Species by Raphidophycean Phytoplankton. *Biosci. Biotechnol. Biochem.* **1997**, *61*, 1658–1662. [CrossRef] [PubMed]
77. Average Separation of Objects within a Volume? 2009. Available online: http://www.forum.cosmoquest.org/showthread.php?93443-Average-separation-of-objects-within-a-volume (accessed on 21 October 2021).
78. Lambert W Function. 2022. Available online: https://en.wikipedia.org/wiki/Lambert_W_function (accessed on 19 January 2022).
79. RC Team. *R: A Language and Environment for Statistical Computing*; R Foundation for Statistical Computing: Vienna, Austria, 2019.
80. RStudio Team. *RStudio: Integrated Development Environment for R.*; RStudio, Inc.: Boston, MA, USA, 2015.
81. Wickham, H.; Averick, M.; Bryan, J.; Chang, W.; McGowan, L.D.; François, R.; Grolemund, G.; Hayes, A.; Henry, L.; Hester, J.; et al. Welcome to the tidyverse. *J. Open Source Softw.* **2019**, *4*, 1686. [CrossRef]
82. Borchers, H.W. Pracma: Practical Numerical Math Functions. 2021. Available online: https://cran.r-project.org/web/packages/pracma/index.html (accessed on 22 October 2021).
83. Wickham, H. *Ggplot2: Elegant Graphics for Data Analysis*; Springer: New York, NY, USA, 2016; ISBN 978-3-319-24277-4.
84. Wilke, C.O. Cowplot: Streamlined Plot Theme and Plot Annotations for 'Ggplot2'. 2019. Available online: https://cran.r-project.org/web/packages/ggplot2/index.html (accessed on 12 December 2021).
85. Kassambara, A. Ggpubr: 'Ggplot2' Based Publication Ready Plots. 2018. Available online: https://cran.r-project.org/web/packages/ggpubr/index.html (accessed on 17 July 2019).
86. Hester, J. Glue: Interpreted String Literals. 2018. Available online: https://cran.r-project.org/web/packages/glue/index.html (accessed on 17 July 2019).
87. Zhu, H. kableExtra: Construct Complex Table with 'Kable' and Pipe Syntax. 2019. Available online: https://cran.r-project.org/web/packages/kableExtra/index.html (accessed on 30 July 2019).
88. Goerg, G.M. LambertW: Probabilistic Models to Analyze and Gaussianize Heavy-Tailed, Skewed Data. 2020. Available online: https://cran.r-project.org/web/packages/LambertW/index.html (accessed on 16 December 2020).
89. Pedersen, T.L. RStudio Ggforce: Accelerating 'Ggplot2'. 2021. Available online: https://cran.r-project.org/web/packages/ggforce/index.html (accessed on 5 March 2021).
90. D'Agostino McGowan, L.; Bryan, J. Googledrive: An Interface to Google Drive. 2020. Available online: https://cran.r-project.org/web/packages/googledrive/index.html (accessed on 21 October 2021).
91. Bryan, J. Googlesheets4: Access Google Sheets Using the Sheets API V4. 2021. Available online: https://cran.r-project.org/web/packages/googlesheets4/index.html (accessed on 21 October 2021).
92. Zotero | Your Personal Research Assistant. Available online: https://www.zotero.org/ (accessed on 7 December 2021).
93. Aust, F. Citr: 'RStudio' Add-in to Insert Markdown Citations. 2018. Available online: https://github.com/crsh/citr (accessed on 17 July 2019).

94. Xie, Y. Knitr: A Comprehensive Tool for Reproducible Research in R. In *Implementing Reproducible Computational Research*; Stodden, V., Leisch, F., Peng, R.D., Eds.; Chapman and Hall/CRC: Boca Raton, FL, USA, 2014. Available online: https://www.taylorfrancis.com/chapters/edit/10.1201/9781315373461-1/knitr-comprehensive-tool-reproducible-research-yihui-xie (accessed on 30 July 2019).
95. Xie, Y. *Dynamic Documents with R and Knitr*; Chapman and Hall/CRC: Boca Raton, FL, USA, 2015. Available online: https://duhi23.github.io/Analisis-de-datos/Yihue.pdf (accessed on 30 July 2019).
96. Xie, Y. Knitr: A General-Purpose Package for Dynamic Report Generation in R; 2018. Available online: https://cran.r-project.org/web/packages/knitr/index.html (accessed on 30 July 2019).
97. Xie, Y. Bookdown: Authoring Books and Technical Documents with R Markdown; 2019. Available online: https://cran.r-project.org/web/packages/bookdown/index.html (accessed on 22 November 2021).